Supplemental Information

The leaf-like structured membrane for highly efficient and persistent radiative cooling

Minghan Wu[#], Yu Li[#], Gang Huang, Ruiqi Xu, Xiaochun Yin, Guizhen Zhang*

1. Key Laboratory of Polymer Processing Engineering of the Ministry of Education, National Engineering Research Center of Novel Equipment for Polymer Processing, Guangdong Provincial Key Laboratory of Technique and Equipment for Macromolecular Advanced Manufacturing, South China University of Technology, Guangzhou 510641, People's Republic of China

2. School of Mechanical and Automotive Engineering, South China University of Technology, Guangzhou 510641, People's Republic of China

* Corresponding to：guizhenzhang@scut.edu.cn

# These authors contributed equally to this work

This PDF file includes:

Supplemental Notes: Note S1 to S5

Supplemental Figures: Figure S1 to S7

Supplemental Tables: Table S1 to S4

Supplemental References

Note S1：Optimization of ultraviolet (UV) reflectivity in the DBPS protective layer by adjusting SiO$_2$ particle radius and content

To theoretically investigate the effects of changes in SiO$_2$ particle radius and solid content on solar reflectivity, this study employed finite-difference time-domain (FDTD) simulations, as shown in Fig. S1. To ensure simulation accuracy, the grid size was set to 0.01 μm. For modeling simplicity, the actual UHMWPE structure was represented by evenly spaced UHMWPE cylinders, with regions outside UHMWPE and SiO$_2$ defined as pore structures. The simulated structure consisted of UHMWPE cylinders with a thickness of 5 μm, a radius of 0.1 μm, and a spacing of 0.5 μm, along with SiO$_2$ particles with a radius of 1 μm.

To analyze the effect of SiO$_2$ particle radius variation, the radius of the SiO$_2$ particles was gradually increased from 0 to 2.5 μm, while the number of SiO$_2$ particles decreased from 157 to 1. This approach was used to simulate the influence of particle radius variation on solar reflectivity. For analyzing the effect of SiO$_2$ solid content variation, the number of SiO$_2$ particles gradually increased from 0 to 10 to simulate the effect of changing solid content on solar reflectivity. The simulations employed perfectly matched layer (PML) boundary conditions and a plane wave light source, with periodic simulations within a 5 × 5 × 8 μm region, yielding theoretical results for reflectivity of the structure.

Note S2：Optimization of UV reflectivity in the DBPS protective layer by adjusting the particle size relationship between the protective and cooling layers

To theoretically investigate the effect of particle size relationship between the

protective and cooling layers on solar reflectivity, FDTD simulations were conducted, as shown in Fig. S2. To ensure simulation accuracy, the grid size was set to 0.01 μm. For modeling simplicity, the actual UHMWPE structure was represented by evenly spaced UHMWPE cylinders, with regions outside UHMWPE and SiO_2 defined as pore structures. The simulated structure consisted of UHMWPE cylinders with a thickness of 10 μm, a radius of 0.11 μm, and a spacing of 0.5 μm, as well as SiO_2 particles with radius of 1 μm and 0.1 μm.

To investigate the relationship of particle size variation between the upper protective layer and the bottom cooling layer, simulations were conducted under two configurations: (1) with the number and radius of SiO_2 particles in the protective layer (upper) fixed at 5 and 1 μm, respectively, and in the cooling layer (bottom) at 445 and 0.1 μm; (2) with the number and radius of SiO_2 particles in the protective layer (upper) fixed at 445 and 0.1 μm, respectively, and in the cooling layer (bottom) at 5 and 1 μm. The simulation utilized PML boundary conditions and a plane wave light source, with periodic simulations within a $10 \times 5 \times 5$ μm region, yielding theoretical results for reflectivity of the structure.

Note S3：Optimization of radiative cooling performance in the DBPS cooling layer

To theoretically investigate the effects of variations in inorganic particle content and the ratio between inorganic particles on solar reflectivity and mid-infrared (MIR) emissivity, FDTD simulations were conducted, as shown in Fig. S6. To ensure simulation accuracy, the grid size was set to 0.01 μm. For modeling simplicity, the

actual UHMWPE structure was represented by evenly spaced UHMWPE cylinders, with regions outside of UHMWPE, SiO₂ and TiO₂ defined as pore structures. The simulated structure consisted of UHMWPE cylinders with a thickness of 8 μm, a radius of 0.11 μm and a spacing of 0.5 μm, along with SiO₂ particles of 1 μm radius and TiO₂ particles of 0.1 μm radius.

In assessing the effect of varying inorganic particle content, the number of SiO₂ particles was increased from 0 to 4, while the number of TiO₂ particles increased from 0 to 3786, simulating the impact of overall SiO₂ and TiO₂ content on solar reflectivity and MIR emissivity. In studying the effects of the content ratio between inorganic particles, the number of SiO₂ particles was gradually increased from 0 to 5, while the number of TiO₂ particles decreased from 2820 to 0, to simulate the influence of SiO₂ to TiO₂ ratio on solar reflectivity and MIR emissivity. The simulations employed PML boundary conditions and a plane wave light source, with periodic simulations within a periodic 8 × 5 × 5 μm region, yielding theoretical results for the reflectivity and emissivity of the structure.

Note S4: Calculations of solar reflectivity and MIR emissivity

To quantify radiative cooling performance, the average solar reflectivity $\bar{R}_{solar}$ and average MIR emissivity $\bar{\epsilon}_{MIR}$ are defined based on the reflectance and emission spectra data as follows.[1]

$$\bar{R}_{solar} = \frac{\int_{0.3\,\mu m}^{2.5\,\mu m} R(\lambda) \cdot I_{AM\,1.5}(\lambda)d\lambda}{\int_{0.3\,\mu m}^{2.5\,\mu m} I_{AM\,1.5}(\lambda)d\lambda} \quad (S6)$$

$$\bar{\epsilon}_{MIR} = \frac{\displaystyle\int_{8\,\mu m}^{13\,\mu m} \epsilon(\lambda) \cdot I_{BB}(\lambda, T)d\lambda}{\displaystyle\int_{8\,\mu m}^{13\,\mu m} I_{BB}(\lambda, T)d\lambda} \qquad (S7)$$

where λ is the wavelength, $R(\lambda)$, $T(\lambda)$ and $\epsilon(\lambda) = 1 - R(\lambda) - T(\lambda)$ are the actual

reflectivity, transmittance and emissivity at wavelength λ, $I_{AM\ 1.5}(\lambda)$ is Normalized AM

1.5 global solar spectrum. Besides, $I_{BB}(\lambda, T) = \dfrac{2hc^2}{\lambda^5} \cdot \dfrac{1}{e^{hc/\lambda K_B T} - 1}$ is the spectral heat

radiance of a blackbody (Planck's law) at temperature T, where h is Planck's constant,

k_B is the Boltzmann constant, and c is the speed of light in vacuum .

Note S5: Calculation of net cooling power

Considering all the energy exchange process, the net cooling power of PRC

material can be calculated as follows:

$$P_{net} = P_{rad} - P_{atm} - P_{solar} - P_{cc} \qquad (S8)$$

Where

$$P_{rad} = \int d\Omega cos\theta \int_0^\infty d\lambda \epsilon_r(\lambda,\theta) I_{BB}(T_r, \lambda) \qquad (S9)$$

is the outward radiation of the radiative cooler,

$$P_{atm} = \int d\Omega cos\theta \int_0^\infty d\lambda \epsilon_r(\lambda,\theta) \epsilon_{atm}(\lambda,\theta) I_{BB}(T_a, \lambda) \qquad (S10)$$

is energy absorption due to atmospheric thermal radiation,

$$P_{solar} = \int_0^\infty d\lambda \epsilon_r(\lambda,0) I_{AM1.5}(\lambda) \qquad (S11)$$

is the solar non-radiative absorption,

$$P_{cc} = h_c(T_{atm} - T_r) \qquad (S12)$$

is non-radiative heat loss due to the convection and conduction.

Here, $\int d\Omega = 2\pi \int_0^{\pi/2} d\theta \sin\theta$ is the angular integral on a hemisphere. $\epsilon_r(\lambda,\theta)$ is the emittance of the radiative cooler at λ. The emittance of the atmosphere is defined by

$\epsilon_{atm}(\lambda,\theta) = 1 - t(\lambda)^{1/\cos\theta}$, where $t(\lambda)$ is the atmospheric transmittance in zenith angle θ. The solar illumination is exhibited by $I_{AM1.5}(\lambda)$, and we assume the structure is facing the sun, thus the zenith angle can be considered as 0. T_r and T_a are the temperature of the radiative cooler surface and atmosphere, respectively, $h_c = h_{conv} + h_{cond}$ is the combined non-radiative heat coefficient ranged from 2–6.9 W·m⁻²·K⁻¹ according to some reports.[2, 3]
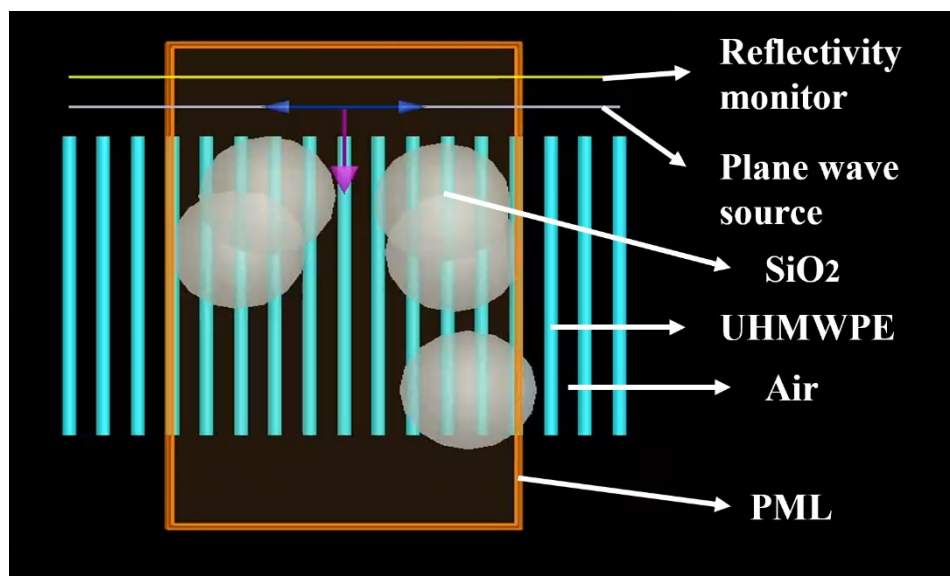
Supplemental Figures

Fig. S1. Schematic of finite-difference time-domain (FDTD) simulation showing the effects of SiO$_2$ particle radius and solid content variations on solar reflectivity. FDTD simulations were conducted to analyze the effect of varying the SiO$_2$ particle radius from 0 to 2.5 μm and the SiO$_2$ solid content from 0 to 80% on the solar reflectivity of a PRC membrane with a protective layer.
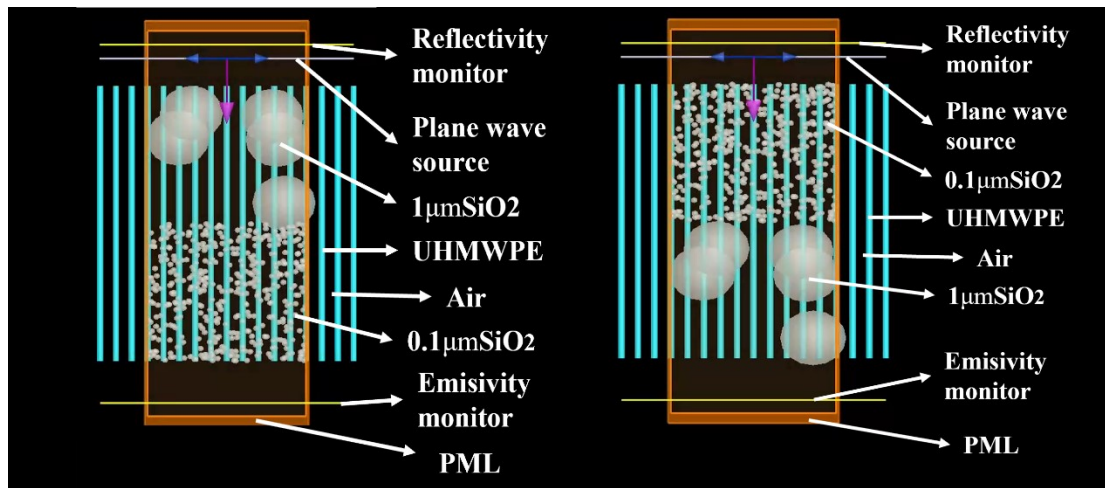
Fig. S2. Schematic of FDTD simulation showing the effects of particle size variations in the upper and bottom layers on solar reflectivity. FDTD simulations were conducted to analyze the impact of transitions from larger particles in the upper layer to smaller particles in the bottom layer, and from smaller particles in the upper layer to larger particles in the bottom layer, on the solar reflectivity of the PRC membrane with a protective layer.

Fig. S3. Continuous production of DBPS using a dual-layer co-extrusion device
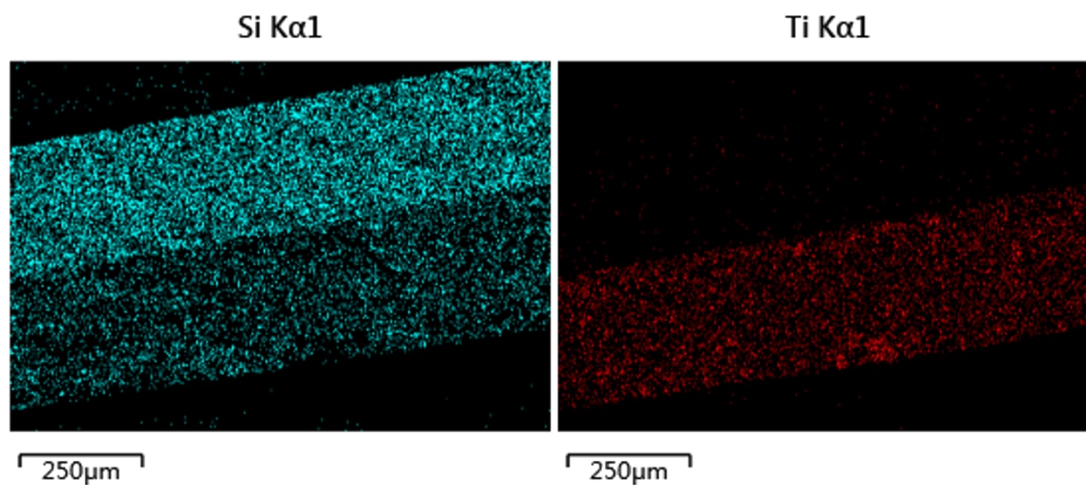
Fig. S4. EDS energy spectrum of DPBS. The left figure displays the elemental mapping of silicon (Si) in the protective and cooling layers, while the right figure shows the elemental mapping of titanium (Ti) in the cooling layer.
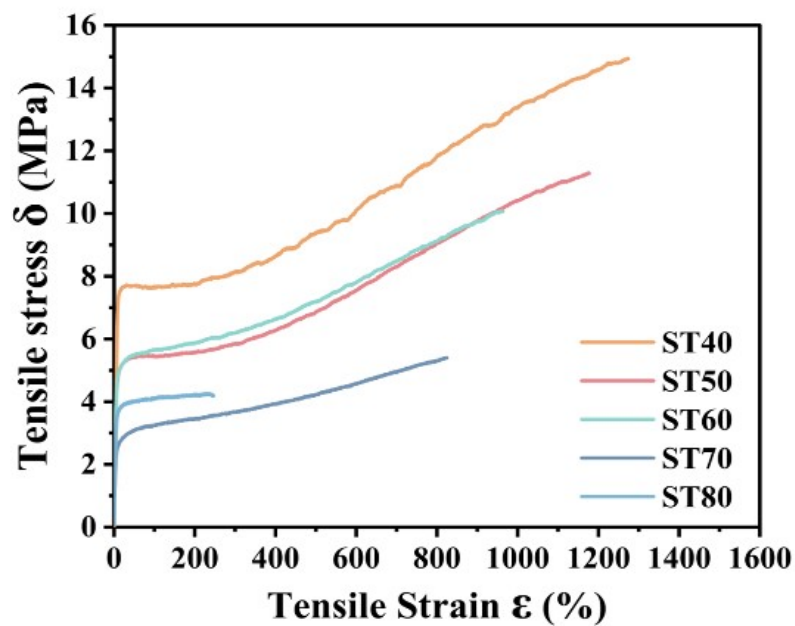
Fig. S5. Stress-strain curves of the PRC membrane under varying total SiO$_2$ and TiO$_2$ content. The addition of SiO$_2$ and TiO$_2$ particles significantly reduces the mechanical performance of the PRC membrane; when the total content of SiO$_2$ and TiO$_2$ reaches 70 wt%, the tensile strength is only 5.2 MPa, and at 80% total content, the tensile strength and elongation at break drop to just 4 MPa and 286%, respectively, making practical application challenging.
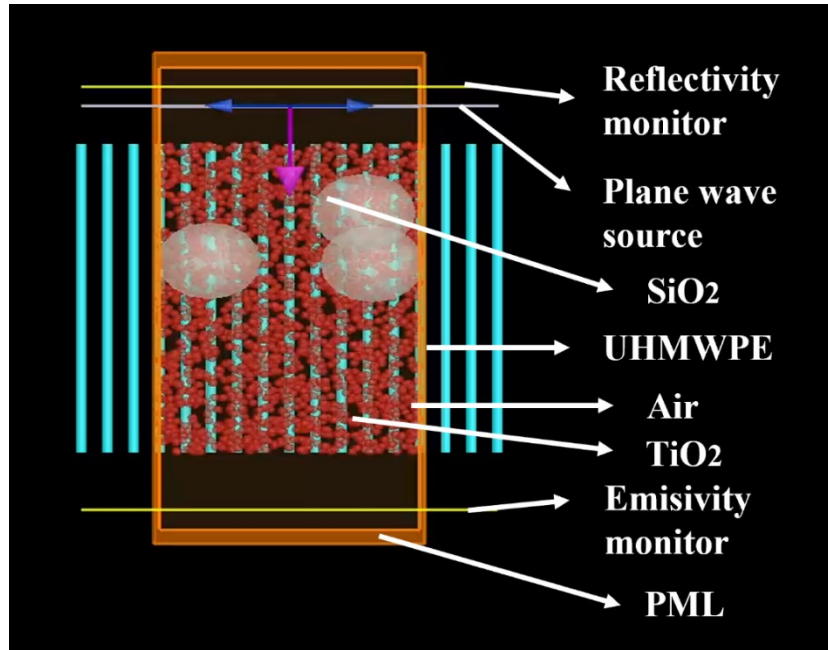
Fig. S6. Schematic of FDTD simulation showing the effects of total SiO$_2$ and TiO$_2$ content variation and the content ratio variation between SiO$_2$ and TiO$_2$ on solar reflectivity and emissivity. FDTD simulations were used to analyze the impact of varying the total SiO$_2$ and TiO$_2$ particle content from 40% to 80%, as well as adjusting the content ratio between SiO$_2$ and TiO$_2$ from 0 to 100% (based on SiO$_2$ variation), on solar reflectivity and mid-infrared (MIR) emissivity.
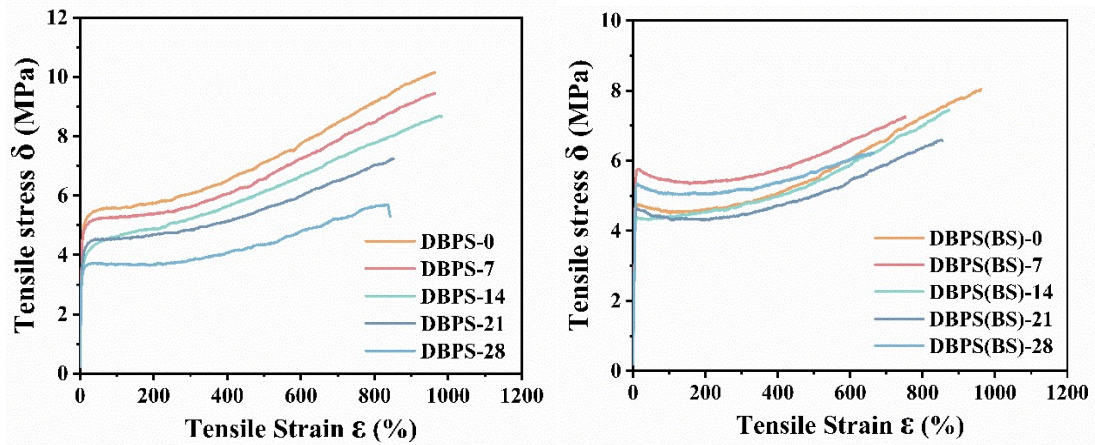
Fig. S7. Stress-strain curves of DBPS (left) and DBPS (BS) (right) under varying durations of UV exposure. Prolonged UV exposure leads to performance degradation in polymer-based microporous membranes, particularly in those containing TiO2 particles, where molecular chain breakage occurs more rapidly. However, polymer-based microporous membranes covered with DBPS maintain exceptional elongation at break, retaining up to 1020% even after 7 days of UV exposure (equivalent to 5 years of outdoor exposure in Guangzhou), with negligible mechanical performance loss. After 28 days of UV exposure (equivalent to 20 years of outdoor exposure in Guangzhou), the elongation at break of DBPS and DBPS (BS) remains at 843.23% and 664.29%, respectively. These results validate the suitability of the DBPS for practical applications under real-world conditions.

Supplemental Tables

Table S1. The average solar reflectivity ($\overline{R}_{solar}$) and average mid-infrared (MIR) emissivity ($\overline{\epsilon}_{MIR}$) of the PRC porous membranes with different SiO_2 and TiO_2 content

Scale	UHMWPE (USD/kg)	LP (USD/kg)	SiO2 (USD/kg)	TiO2 (USD/kg)	Total cost (USD/m2)
Laboratory scale	1.71	11.39	33.94	36.53	9.49
Industrial scale	1.71	1.23	1.64	2.05	0.89

Producing 1 kg of DBPS gel requires 92.31 g of silicon dioxide (SiO_2), 138.46 g of titanium dioxide (TiO_2), 153.85 g of ultra-high molecular weight polyethylene (UHMWPE), and 615.38 g of liquid paraffin (LP). From 1 kg of DBPS gel, membranes with a thickness of 350 μm and a total area of 1.63 m^2 can be fabricated. Based on this information, the production costs for laboratory scale and industrial scale manufacturing were calculated as follows:

For laboratory scale production, the following materials prices were considered: UHMWPE (viscosity-average molecular weight, 1.8×10^6 g/mol, supplier: Shanghai Chemical Research Institute; price: 1.71 USD/kg), LP (supplier: Aladdin; price: 11.39 USD/kg), SiO_2 (supplier: Macklin; price: 33.94 USD/kg), and TiO_2 (supplier: Macklin; price: 36.53 USD/kg). Based on these prices, the total production cost was calculated to be 9.49 USD/m^2.

For industrial scale production, manufacturers capable of providing large quantities of materials at reduced costs were selected: UHMWPE (viscosity-average

molecular weight, 1.8×10^6 g/mol, supplier: Shanghai Chemical Research Institute; price: 1.71 USD/kg), LP (supplier: Zhejiang Zhengxin Petroleum Technology Co., Ltd.; price: 1.23 USD/kg), SiO_2 (supplier: Hoshine Silicon Industry Co., Ltd.; price: 1.64 USD/kg), and TiO_2 (supplier: LB Group Co., Ltd.; price: 2.05 USD/kg). Based on these prices, the total production cost was calculated to be 0.89 USD/m^2. The production costs for laboratory scale and industrial scale manufacturing are detailed in Table S1.

Table S2. The average solar reflectivity ($\bar{R}_{solar}$) and average mid-infrared (MIR)

emissivity ($\bar{\epsilon}_{MIR}$) of the PRC porous membranes with different SiO_2 and TiO_2 content

Samples	Theoretical thickness/mm	Actual thickness/μm	$\bar{R}_{solar}$/%	$\bar{\epsilon}_{MIR}$/%	$\bar{R}_{MIR}$/%	T_{MIR}/%
ST40		350	94.1	92.5	5.7	1.8
ST50		350	94.5	93.0	6.9	0.1
ST60	0.5	350	96.1	95.1	4.9	0
ST70		350	95.4	95.3	4.7	0
ST80		350	91.5	95.5	4.5	0

Table S3. The average solar reflectivity ($\bar{R}_{solar}$) and average MIR emissivity ($\bar{\epsilon}_{MIR}$) of the PRC porous membranes with different SiO_2 and TiO_2 content ratios

Samples	Theoretical thickness/mm	Actual thickness/μm	$\bar{R}_{solar}$/%	$\bar{\epsilon}_{MIR}$/%	$\bar{R}_{MIR}$/%	T_{MIR}/%
T60		350	94.6	91.5	5.1	3.4
ST60-1/4		350	94.7	93.9	6.1	0
ST60-2/3		350	96.1	95.1	4.9	0
ST60-3/2	0.5	350	95.4	93.3	6.7	0
ST60-4/1		350	94.9	92.5	7.5	0
S60		350	96.6	90.4	8.9	0.6

Table S4. The average solar reflectivity ($\bar{R}_{solar}$) and solar reflectivity across different wavelength bands (280–2500 nm) of DBPS.

Samples	Theoretical thickness/mm	Actual thickness/μm	$\bar{R}_{solar}$ /%	280–400nm /%	400–700nm /%	700–2500nm /%
DBPS	0.5	350	99.3	106.8	101.5	95.9

Supplemental References

1. J. Mandal, Y. K. Fu, A. C. Overvig, M. X. Jia, K. R. Sun, N. N. Shi, H. Zhou, X. H. Xiao, N. F. Yu and Y. Yang, *Science*, 2018, **362**, 315-318.
2. A. P. Raman, M. A. Anoma, L. Zhu, E. Rephaeli and S. Fan, *Nature*, 2014, **515**, 540-544.
3. M. M. Hossain and M. Gu, *Advanced Science*, 2016, **3**, 1500360.